Fractional Chern insulator phase at the transition between checkerboard and Lieb lattices

Błażej Jaworowski,[1,*] Andrei Manolescu,[2] and Paweł Potasz[1]
[1]*Department of Theoretical Physics, Wroclaw University of Technology, Wybrzeze Wyspianskiego 27, 50-370 Wroclaw, Poland*
[2]*School of Science and Engineering, Reykjavik University, Menntavegur 1, IS-101 Reykjavik, Iceland*
(Received 22 August 2015; published 14 December 2015)

The stability of the $\nu = 1/3$ fractional Chern insulator (FCI) phase is analyzed on the example of a checkerboard lattice undergoing a transition into a Lieb lattice. The transition is performed by the addition of a second sublattice, whose coupling to the checkerboard sites is controlled by sublattice staggered potential. We investigate the influence of these sites on the many-body energy gap between three lowest energy states and the fourth state. We consider cases with different complex phases acquired in hopping and a model with a flattened topologically nontrivial band. We find that an interaction with the additional sites either open the single-particle gap or enlarge the existing one, which translates into similar effect on the many-particle gap. By looking at Berry curvature flatness we notice its strong correlation with the magnitude of the many-body energy gap, suggesting that the main mechanism of the FCI stabilization by additional atoms is via their influence on the Berry curvature. Evidence of the FCI phase for a region in a parameter space with larger energy gap is shown by looking at momenta of the threefold degenerate ground state, spectral flow, and quasihole excitation spectrum.

DOI: 10.1103/PhysRevB.92.245119 PACS number(s): 73.43.−f, 71.10.Fd, 03.65.Vf

Recent work on fractional Chern insulators (FCIs) as a lattice version of fractional quantum Hall effect (FQHE) [1,2] without a need of Landau levels has attracted significant attention [3–12]. Those are many-particle extensions of Chern insulators [13]—systems which exhibit integer quantum Hall effect without magnetic field and were recently realized experimentally [14,15]. FCIs are particularly interesting because they can mimic Landau level physics and may provide a more convenient way of conducting experiments on FQHE, as they can exist in higher temperatures and would not need high magnetic fields [4]. FCIs can also depart from Landau level physics, which happens, e.g., for bands with Chern numbers higher than 1, where new forms of FCI states can arise [16–19].

Experimental realizations of the FCI phase were proposed in different systems including cold atoms [20] or molecules in optical lattices [21,22], graphene [23–25], arrays of quantum wires [26], transition-metal oxide heterostructures [27,28], or strongly correlated electrons in layered oxides [29–31].

Initially, it was proposed that FCIs should exist on topologically nontrivial flat band models [3,4,18,32–34]. Several lattice models with quasiflat topologically nontrivial bands have been shown numerically to exhibit the FCI phase, including checkerboard [5–8,35], honeycomb [6,36], square [36], triangular [29], and kagome lattices [36]. Numerical evidence for analogs of a number of FQHE states, including Laughlin $1/m$ [5], composite fermion hierarchy [9,37], and non-Abelian Moore-Read and Read-Rezayi states [36,38,39] was found. For bands with higher Chern numbers, states with no direct analog in FQHE were found, some of which exhibited non-Abelian statistics [16,17,19].

To prove the existence of FCIs in torus geometry for filling p/q one should show q quasidegenerate ground states [40–42], which flow into each other and do not intersect with higher states when one flux quantum is inserted through a handle of the torus [42–44], and obey the momentum counting rules [38,41]. These rules need to be satisfied also for quasihole excitations [8,36]. Alternative methods of proving FCI existence include many-body Chern number [5,42,44] and entanglement spectrum [8,45–47].

There are several criteria which allow one to find systems which can host the FCI phase. First, the flatness ratio (a ratio of magnitude of band dispersion to the energy gap) needs to be low, to maximize the effect of interaction. However, this criterion has proven ambiguous, as the single-particle dispersion can stabilize the FCI phase [9,29,48–50], and interactions far exceeding band gap do not always lead to the destruction of FCIs [51]. Secondly, in the limit of long wavelength and uniform Berry curvature, the projected density operator algebra resembles the Girvin-MacDonald-Platzman algebra [52] for a Landau level. In consequence an energy band needs to have nearly-flat Berry curvature to host the FCI phase [36,53]. Also, a third criterion, based on the Fubini-Study metric was proposed recently [54–56]. However, clear conditions for FCI existence are not perfectly understood.

In this work, we want to investigate how the stability of FCIs on a given lattice is affected by introducing an interaction with extra lattice sites. We consider a checkerboard lattice which transforms into a Lieb lattice [57–61] when a second sublattice is introduced into the system, controlled by on-site staggered potential. We investigate the transition between two lattices in the context of the FCI phase for spinless particles for $1/3$ filling. For finite-size systems in a torus geometry, we analyze the influence of the interaction between the two sublattices on the many-body energy gap between three lowest energy states and the fourth state. For a specific choice of parameters corresponding to an area of larger energy gap, we search for signatures of $1/3$ Laughlin-like phase. Three lowest energy states (a threefold ground state manifold) are analyzed with respect to (i) their momenta, (ii) the energy gap to excited states for different system sizes, and (iii) spectral flow. Also, the quasihole spectrum and its momentum counting is investigated. Our results suggest the existence of the FCI phase with a stability supported by the interaction with extra lattice sites. The main mechanism responsible for this is the influence of extra sites on Berry curvature. The paper

*blazej.jaworowski@pwr.edu.pl

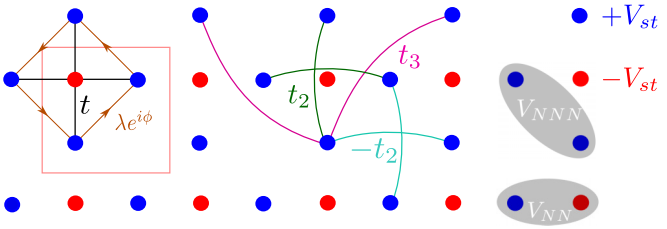

(a)

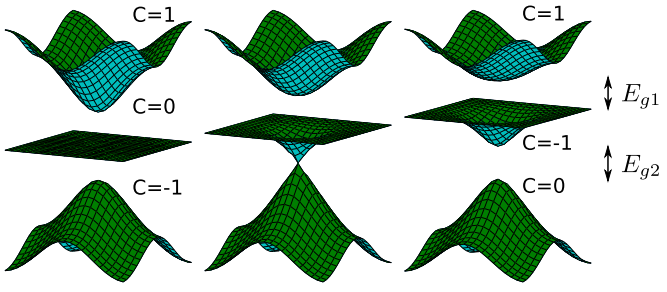

(b)

FIG. 1. (Color online) (a) Structure of Lieb lattice. Red and blue atoms belong to sublattices A and B, respectively. Solid black lines denote real nearest-neighbor hoppings; arrows denote complex second-neighbor hoppings. Other solid lines denote further-neighbor hoppings used to flatten the middle band. t_2 hopping connects the second-nearest neighbors within the B sublattice, if an A atom is between them. Otherwise, the hopping is $-t_2$. t_3 hoppings connect third-nearest neighbors within the B sublattice. Gray ellipses denote interaction parameters. (b) Topological phase transition in the Lieb lattice.

is organized as follows: in Section I we describe the lattice model, Sec. II contains a single-particle analysis, in Sec. III many-body effects are investigated, and in Sec. IV we conclude our results.

I. MODEL

A face centered two-dimensional square lattice called a Lieb lattice is considered, shown in Fig. 1(a). The lattice can be divided into two sublattices A and B, distinguished in Fig. 1(a) by red and blue colors. We use tight-binding Hamiltonian

$$H = t\sum_{\langle i,j\rangle} c_i^\dagger c_j + \lambda \sum_{\langle\langle i,j\rangle\rangle} e^{i\phi_{ij}} c_i^\dagger c_j + V_{st}\sum_{i\in A} c_i^\dagger c_i - V_{st}\sum_{i\in B} c_i^\dagger c_i, \quad (1)$$

where in the first term $\langle\,\rangle$ denotes summation over nearest neighbors with the hopping integral t, the second term is a next-nearest-neighbor term denoted by $\langle\langle\,\rangle\rangle$ with hopping amplitude λ and an accumulated extra complex phase $\phi_{ij} = \pm\phi$ when going clockwise and counterclockwise, respectively, and V_{st} is a staggered sublattice potential. We note that for $\phi = \pi/2$ the second term corresponds to Kane-Mele spin-orbit coupling [62], and $\phi = \pi/4$ was considered for a checkerboard lattice in Refs. [3,5]. In the latter case, extra hoppings were added to open the gap and flatten one of the bands; they are shown as t_2 and t_3 in Fig. 1(b), with values $t_2 = \frac{\lambda}{2+\sqrt{2}}$ and $t_3 = \frac{\lambda}{2+2\sqrt{2}}$ [3,5]. A transition between a Lieb lattice and a checkerboard lattice is driven by tuning V_{st} to infinity. In this case, lattice sites represented in red in Fig. 1(b) are decoupled from sites represented in blue, and systems consisting of sites of different colors can be treated independently, with blue sites forming a checkerboard lattice. A systematic analysis of this transition will be presented in the next section.

Many-body effects are studied using density-density interaction of the form

$$V = V_{NN}\sum_{\langle i,j\rangle} n_i n_j + V_{NNN}\sum_{\langle\langle i,j\rangle\rangle} n_i n_j, \quad (2)$$

where n_i is a density operator on site i, and V_{NN} and V_{NNN} are interactions between first and second neighbors, respectively. We will focus on correlation effects within the middle band, so the Hilbert space is truncated, containing states from this band only. The lower band is considered as completely filled. Also, a flat-band approximation is used neglecting the kinetic energies. We note that middle band states are localized mostly on one sublattice [indicated by blue in Fig. 1(b)] even for low V_{st}, as long as it is topologically nontrivial. Therefore, the leading term in Eq. (2) is between second neighbors, V_{NNN}. All calculations are performed for finite-size $N_x \times N_y$ samples with a torus geometry, where N_x (N_y) is a number of unit cells in x (y) direction. We consider 1/3 filling of the middle band which corresponds to $N = N_x N_y/3$ particles in the system. Due to a translation symmetry and momentum conservation of two particle Coulomb scattering term, many-body eigenstates can be indexed by total momentum quantum numbers K_x and K_y, which are the sum of the momentum quantum numbers of each of the N particles modulo N_x and N_y, respectively.

II. SINGLE-PARTICLE ANALYSIS

The unit cell of the Lieb lattice consists of three sites giving three energy bands after diagonalization of the Hamiltonian given by Eq. (1). A band structure in the simplest case when only nearest-neighbor hopping integrals t are included has the lower and upper bands touching each other in the middle of the energy spectrum at energy $E = 0$, where the perfectly flat third energy band is present [59]. Two dispersive bands are almost equally localized on both sublattices, while the flat middle band is almost fully localized on a sublattice indicated in blue in Fig. 1(a). We next introduce the second term from Eq. (1) with $\phi = \pi/2$. The energy gap opens and the lower and upper bands are topologically nontrivial with Chern numbers $C = -1$ and $C = 1$, respectively, and the middle flat band is topologically trivial with Chern number $C = 0$, as shown in Fig. 1(b) on the left. Following Zhao and Shen [60], the topology of the energy bands can be changed by introducing a staggered sublattice potential, i.e., the two last terms in the Hamiltonian given by Eq. (1). An increase of V_{st} leads to bending of the middle band. At a critical value of $V_{st} = 2\lambda$, the middle and lower bands touch [see the band structure shown in the middle in Fig. 1(b)]. At this point a topological phase transition occurs. For $V_{st} > 2\lambda$, the lower band becomes topologically trivial with Chern number $C = 0$, while the middle band becomes nontrivial with Chern number $C = -1$, which is shown in Fig. 1(b) on the right. A similar transition occurs for $\phi = \pi/4$,

but at the value $V_{st} = \sqrt{2}\lambda$ and at $V_{st} = \lambda$ when t_2 and t_3 are considered.

Two energy gaps are indicated in Fig. 1(b) on the right: E_{g_1} between two topologically nontrivial bands, the upper ($C = 1$) and the middle band ($C = -1$), and E_{g_2} between topologically nontrivial middle band ($C = -1$) and topologically trivial lower band ($C = 0$). We investigate a magnitude of these gaps as a function of model parameters. In Fig. 2(a), a schematic evolution of the energy bands as a function of a staggered sublattice potential V_{st} for $\lambda = 0.2$ and $\phi = \pi/2$ is shown. An increase of V_{st} increases E_{g_2}, separating two topologically nontrivial higher energy bands from the lower band. This corresponds also to decoupling of a sublattice indicated in red from a sublattice indicated in blue in Fig. 1(a). In a limit of $V_{st} \to \infty$, two sublattices are completely decoupled and the Lieb lattice transforms into the checkerboard lattice [blue sites in Fig. 1(b)]. At the same time, the energy gap E_{g_1} between two topologically nontrivial bands from the checkerboard lattice decreases monotonically to zero. A map of a magnitude of the energy gap E_{g_1} as a function of the staggered sublattice potential V_{st} and λ for $\phi = \pi/2$ is shown in Fig. 2(b). The staggered sublattice potential V_{st} is varied from $V_{st} = 0$ to $V_{st} \to \infty$, which can be performed by introducing a parameter s given by a formula $V_{st} = 4\tan(s\pi/2)$, where s changes in a range of values $s = (0,1)$. For an isolated checkerboard lattice corresponding to $s = 1$ ($V_{st} \to \infty$), $E_{g_1} = 0$. An introduction of finite V_{st} opens the energy gap E_{g_1}.

For sufficiently high V_{st} the energy gap is a direct gap in M point of the Brillouin zone, with magnitude $E_{g1} = \sqrt{4t^2 + V_{st}^2} - V_{st}$. Below $V_{st} = \frac{t^2}{2\lambda} - 2\lambda$ [white line in Fig. 2(b)] the bottom of the highest band is located at

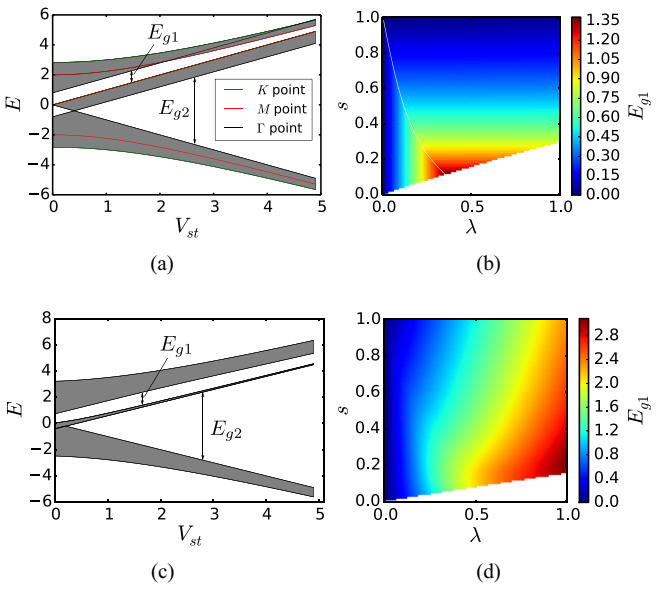

FIG. 2. (Color online) (a), (c) Evolution of the band structure of the Lieb lattice in a function of V_{st} for fixed $\lambda = 0.2$. (b), (d) Maps of single-particle energy gap E_{g1} depending on λ and staggered potential V_{st}, parametrized by $V_{st} = 4\tan(s\pi/2)$. The top and bottom rows correspond to $\phi = \pi/2$ and $\phi = \pi/4$, respectively. The white line in (b) shows the border between the direct (above the line) and indirect (below the line) gaps between the upper and middle bands.

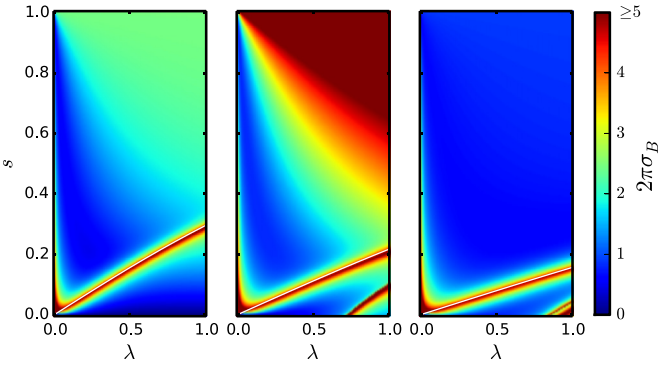

FIG. 3. (Color online) Maps of the standard deviation of Berry curvature σ_B (in the units $\frac{1}{2\pi}$), in functions of parameters λ and s [where $V_{st} = 4\tan(s\pi/2)$], for $\phi = \pi/2$ (left), $\phi = \pi/4$ without additional hoppings (middle), and $\phi = \pi/4$ with a middle band flattened by additional hoppings (right). The white lines denote the topological phase transition at $V_{st} = 2\lambda$ for $\phi = \pi/2$, at $V_{st} = \sqrt{2}\lambda$ for $\phi = \pi/4$ without additional hoppings, and $V_{st} = \lambda$ for $\phi = \pi/4$ with additional hoppings.

the Γ point, therefore E_{g1} is an indirect gap of magnitude 4λ. We note that the bandwidth of the middle band in the topologically nontrivial region is also 4λ, so the flatness ratio of the middle band is $\leqslant 1$. The energy gaps for phase $\pi/4$ show similar behavior, although closed-form expression for E_{g1} for high V_{st} cannot be obtained. On the other hand, for $\phi = \pi/2$ and $V_{st} \to \infty$ the bands touch at the whole boundary of the Brillouin zone (hence the energy of highest band at both M and K points asymptotically approach the top of the middle band), while for $\phi = \pi/4$ the gap is closed only at the M point.

If additional hoppings are included for $\phi = \pi/4$ [Figs. 2(c) and 2(d)], the top of the middle band is not located in any high-symmetry point, therefore E_{g1} can be obtained only numerically. In Fig. 2(c) we show the dependence of energy gaps on V_{st} for $\lambda = 0.2$. Similarly to the previous case, E_{g2} increases to infinity with increased V_{st}. However, contrary to the previous case, in the $V_{st} \to \infty$ limit E_{g1} remains finite (as was noted in Ref. [3], additional hoppings open the gap for the checkerboard model). As shown in Fig. 2(d), the value of this gap depends on λ, which is the only single-particle energy scale in $V_{st} \to \infty$ limit. We note that E_{g1} for given λ has maximum for finite V_{st} [Fig. 2(d)], e.g., at $s \approx 0.3$ for $\lambda = 0.2$. Therefore the additional atoms increase the energy gap, which may be beneficial for the stability of FCI states.

As was shown in Refs. [36,53], Berry curvature flatness has a positive effect on FCI stability. Motivated by this fact, we investigate the standard deviation of Berry curvature σ_B of the middle band of our model. The results are shown in Fig. 3. For $\phi = \pi/2$ and $\phi = \pi/4$ without additional hoppings (right and middle subplots of Fig. 3, respectively), there is a nearly triangular region of low σ_B, with minimum located at finite V_{st}. In this area, an emergence of the FCI phase can be expected. If additional hoppings are included, the Berry curvature has low standard deviation for almost all λ and V_{st} values for which the system is topologically nontrivial. Although the variation of σ_B is too small to be seen in the graph, the minimum of σ_B for fixed λ lies at finite V_{st}. This indicates a small but positive effect of additional atoms on the stability of the FCI phase.

III. MANY-BODY RESULTS

A. The transition between Lieb and checkerboard lattices

The staggered sublattice potential V_{st} controls the energetic distance between sites forming a checkerboard lattice [indicated in blue in Fig. 1(b)] and extra sites [indicated in red in Fig. 1(b)] introduced to create the Lieb lattice. Analyzing the existence of a Laughlin-like phase during the transition between two lattices, we look at the magnitude of the energy gap between threefold degenerate ground states and the fourth state. We perform calculations on a (4×6) torus for interaction parameters $V_{NN} = 1.5$ and $V_{NNN} = 1$. The energy spectra are calculated using an exact diagonalization method, employing either a Lanczos method or the PRIMME package [63].

Despite the flatness ratio not exceeding 1, flat-band approximation [5,36] is applied as a first approximation, to focus only on the effects of interaction, neglecting the effects of single-particle dispersion and mixing with other bands. In our calculations, we assume the lower band is completely filled and the middle band is filled in 1/3. We have verified the validity of neglecting excitations from the lower band checking that they do not significantly affect the many-body energy of the three lowest states. We only noticed some effect of electrons from the lower band close to a single-particle topological phase transition, where results should be treated tentatively.

We first consider the situation for $\phi = \pi/2$ in the second term of the Hamiltonian given by Eq. (1). Figure 4 on the left shows a map of the energy gap as a function of λ and a staggered sublattice potential, represented by the parameter s. A single-particle topological phase transition is marked by a white line in the graph, with a topologically nontrivial region above the line. Opening of the energy gap coincides with single-particle topological phase transition for $V_{st} = 2\lambda$, similarly to results from Ref. [8]. Within a topologically nontrivial region the energy spread δ of threefold degenerate ground state does not exceed $\delta = 0.015$. Therefore, in a major part of this region threefold degenerate ground state separated by the gap is clearly seen in the energy spectrum. Values of the parameter $s \approx 1$ ($V_{st} \to \infty$) correspond to an isolated checkerboard lattice giving the energy gap $E_{gap} \approx 0.02$. However, for infinite staggered potential, $s = 1$, the energy gap $E_{g1} = 0$, and the validity of the results is uncertain because one cannot restrict calculations to one band only when the gap closes. Also, for s close to 1 the spread of three states becomes comparable with energy gap, therefore their quasidegeneracy is not visible. For smaller values of a parameter s, a region with an increased energy gap appears (a red area in Fig. 4), with the largest energy gap $E_{gap} \approx 0.08$ for $\lambda \approx 0.1$ and the parameter $s \approx (0.3,0.7)$ [$V_{st} \approx (2.0,8.0)$]. Thus, an interaction with extra sites, along with opening a single-particle gap, stabilizes the FCI phase. Interestingly, the maximum values of the many-particle gap coincide with the white line in Fig. 2(b)–the transition between the indirect and direct gaps.

In Fig. 4 on the right a phase diagram for a phase $\phi = \pi/4$ is shown. There are no significant qualitative differences comparing to results for $\phi = \pi/2$. Quantitatively, the magnitude of the many-particle gap is smaller than for $\phi = \pi/2$. Also, the region of increased gap is slightly bigger than for $\phi = \pi/2$, because the topological phase transition occurs at $V_{st} = \sqrt{2}\lambda$ instead of $V_{st} = 2\lambda$.

In Fig. 5, a phase diagram for $\phi = \pi/4$ with a flattened middle band is shown. This corresponds to a map of the single-particle energy gap E_{g1} from Fig. 2(d). Within a major part of the range of parameters, the energy gap is approximately constant and larger in comparison to the energy gaps for nonflattened bands from Fig. 4, with a maximum of $E_{gap} \approx 0.085$. The single-particle gap E_{g1} remains open in

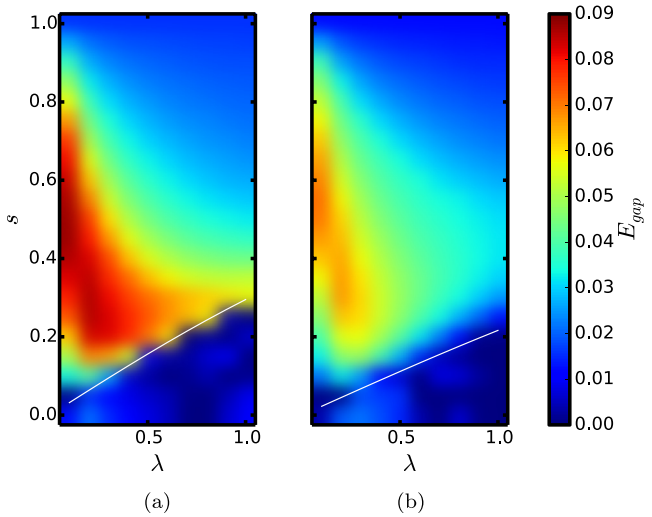

FIG. 4. (Color online) A map of the energy gap between the third and fourth state for a nonflattened middle band with (a) phase $\phi = \pi/2$ and (b) phase $\phi = \pi/4$ (right) as a function of a parameter λ and a staggered sublattice potential V_{st} parametrized by $V_{st} = 4\tan(s\pi/2)$. Interaction strengths are $V_{NN} = 1.5$, $V_{NNN} = 1$. The white line denotes the single-particle topological phase transition for $V_{st} = 2\lambda$ for $\phi = \pi/2$ and $V_{st} = \sqrt{2}\lambda$ for $\phi = \pi/4$.

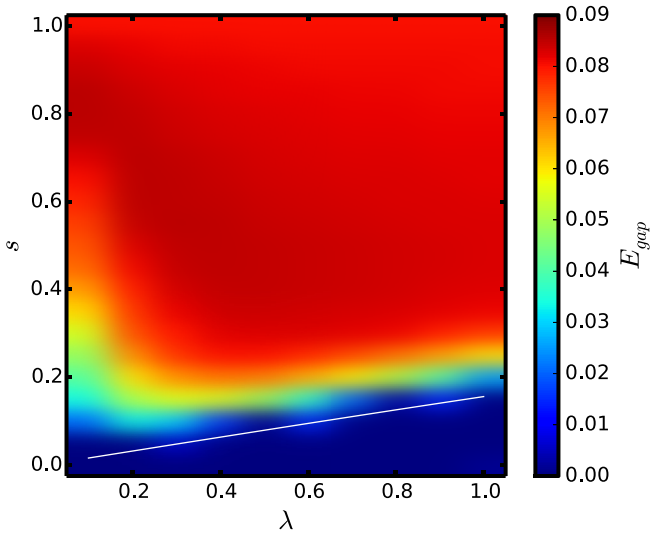

FIG. 5. (Color online) A map of the energy gap between the third and fourth state for a middle band flattened using additional hoppings t_2 and t_3, for a phase $\phi = \pi/4$, as a function of a parameter λ and a staggered sublattice potential V_{st} parametrized by $V_{st} = 4\tan(s\pi/2)$. Interaction strengths are $V_{NN} = 1.5$, $V_{NNN} = 1$. The white line denotes the single-particle topological phase transition.

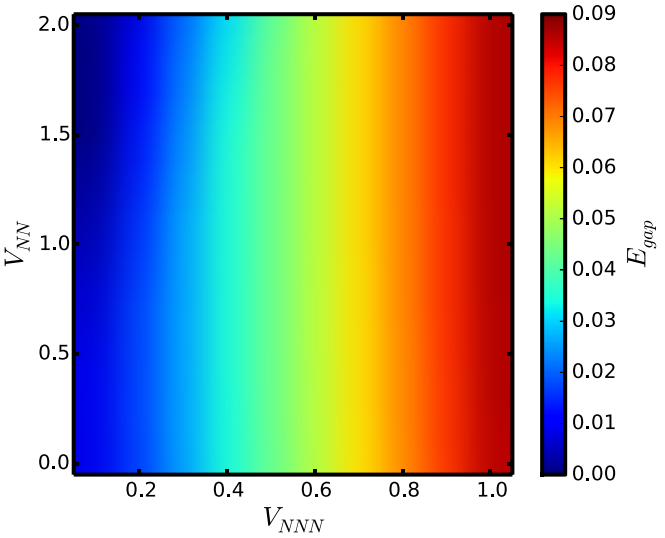

FIG. 6. (Color online) A map of the energy gap between the third and fourth state as a function of interaction parameters V_{NN} and V_{NNN} for $\phi = \pi/2$, $\lambda = 0.2$, $V_{st} = 2$.

the limit $V_{st} \to \infty$. The finite value of the many-particle gap in this limit agrees with earlier results for the checkerboard model [5,8]. No gap closing for finite V_{st} shows that the FCI on the Lieb lattice with additional hoppings is adiabatically connected to that on the checkerboard lattice. A decrease of the energy gap E_{gap} is only seen for $\lambda \approx 0.1$ and close to a single-particle topological phase transition ($V_{st} = \lambda$) marked by a white line.

For all three considered models, a strong correlation between FCI stability and the Berry curvature flatness is observed. The regions of high many-body gap in Figs. 4 and 5 coincide with the regions of small standard deviations of Berry curvature in Fig. 3. This agrees with the results connecting σ_B with FCI stability [36,53]. Thus, we conclude that the main mechanism of FCI stabilization by additional atoms is their influence on Berry curvature.

In Fig. 6 we show the dependence of the energy gap between threefold-degenerate ground state and the fourth states on interaction parameters for fixed $\lambda = 0.2$ and $V_{st} = 2$. In general, the energy gap scales approximately linearly with an interaction between next-nearest neighbors V_{NNN} [an interaction between particles occupying blue sites in Fig. 1(a)] and only slightly depends on V_{NN} [an interaction between particles occupying sites with different colors in Fig. 1(a)]. This is related to the fact that for this choice of parameters the states from the middle band are 98% localized within the sublattice forming a checkerboard lattice [blue sites in Fig. 1(a)].

B. Identification of FCI phase

The correlation between the standard deviation of Berry curvature and the many-body energy gap strongly suggest that the many-body ground state in the red regions in Figs. 4 and 5 is the FCI state. However, this claim needs further confirmation. Thus, for chosen parameters from such a region, $\lambda = 0.2$ and $V_{st} = 2$, and phase $\phi = \pi/2$, we investigate signatures of

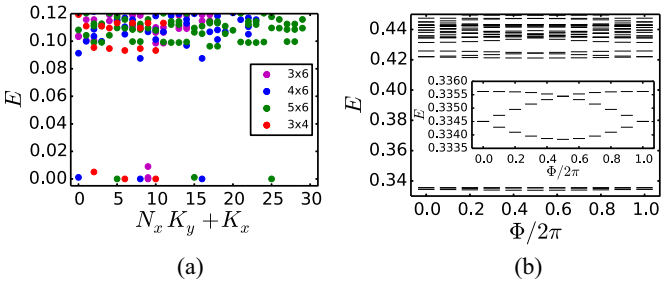

FIG. 7. (Color online) (a) Momentum-resolved low energy spectra for systems with different sizes given by $(N_x \times N_y)$ for parameters $\phi = \pi/2$, $\lambda = 0.2$, $V_{st} = 2$, $V_{NN} = 1.5$, and $V_{NN} = 1$. The energy is rescaled so that ground state energy is set to 0. The momenta of three quasidegenerate states agree with a counting rule for FCI. (b) Spectral flow upon flux insertion for a (4×6) lattice. The threefold degenerate ground states flow into each other and do not cross with higher energy states. The inset shows a magnified view of the ground state manifold evolution.

a 1/3 Laughlin-like state. Figure 7(a) shows a momentum-resolved energy spectrum for different torus sizes. The energy spectra are plotted with respect to the ground state energy at $E = 0$. We find that for each system size we have a threefold quasidegenerate ground state, whose momentum counting corresponds to that obtained from generalized Pauli principle [8]. In the case of $N_x \times N_y = (4 \times 6)$ this corresponds to total momenta of three quasidegenerate ground states for momenta (K_x, K_y): (0,0), (0,2), and (0,4). The electron density of the ground state manifold is almost uniformly distributed within sublattice B, as expected for the incompressible liquid. Small variations can be attributed to finite-size effects. In Fig. 7(b) the spectral flow upon magnetic flux insertion for a (4×6) torus is shown. The threefold degenerate ground states do not intersect with higher states. Three states flow into each other and return to themselves after insertion of three magnetic fluxes.

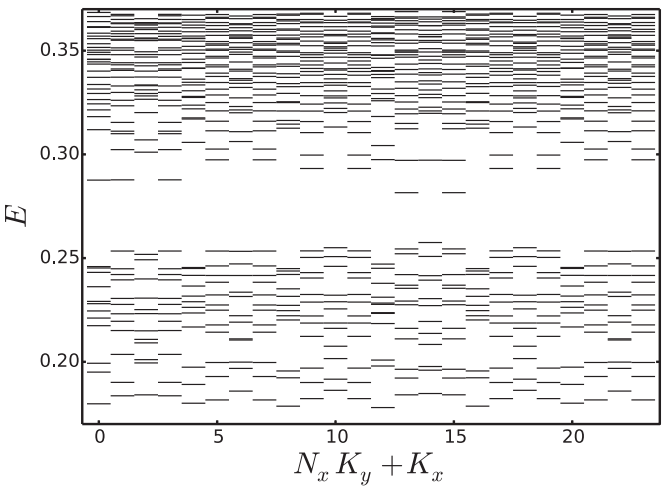

FIG. 8. Momentum-resolved energy spectrum for $N = 7$ electrons on a (4×6) torus for parameters $\phi = \pi/2$, $\lambda = 0.2$, $V_{st} = 2$, $V_{NN} = 1.5$, and $V_{NN} = 1$. The number of states below the gap starting around $E = 0.25$ is 12 for each momentum sector. This is in agreement with counting for Laughlin quasihole states.

This no-mixing property of the ground state manifold with higher energy states is necessary but not sufficient to prove the existence of a Laughlin-like phase. Thus, we analyze quasihole excitations from this state [8,36]. Figure 8 shows quasihole spectra for $N = 7$ electrons on a (4×6) torus (three quasiholes). In this case, 12 quasihole states per momentum sector for Laughlin-like excitations is predicted. This is indeed observed in Fig. 8. Similarly, the results for a (5×5) torus filled by eight electrons (one quasihole) also obeys the counting rules. The spectrum is divided into two parts separated by a clear energy gap, with 12 quasihole states per momentum sector below the gap (not shown). Thus, our results strongly suggest the presence of a FCI in this system.

IV. CONCLUSIONS

In summary, we have analyzed the transition between a checkerboard lattice and a Lieb lattice in the context of the FCI phase for 1/3 filling of a topologically nontrivial energy band. Results were presented for two different complex phases, and a model with a flattened topologically nontrivial band. For the nonflattened bands, the additional sites open the single-particle energy gap and allow a FCI to exist. For a flattened band, they increase the single-particle energy gap and stabilize the FCI. We find that the main stabilizing effect of additional atoms is their influence on Berry curvature, as we find a strong connection between its flatness and the magnitude of the many-body energy gap. The existence of FCI is proven by topological degeneracy, spectral flow, and momentum counting, both for exact 1/3 filling and systems with quasiholes. The topologically nontrivial character of the FCI phase is also seen by the fact that it exists only in parameter regions corresponding to a single-particle topologically nontrivial band.

ACKNOWLEDGMENTS

We thank T. Neupert for very constructive remarks and suggestions regarding the identification of the FCI phase. The authors acknowledge partial funding from the Iuventus Plus program of the Polish Ministry of Science and Higher Education (Grant No. IP2012 007372).

[1] D. C. Tsui, H. L. Stormer, and A. C. Gossard, Phys. Rev. Lett. **48**, 1559 (1982).
[2] R. B. Laughlin, Phys. Rev. Lett. **50**, 1395 (1983).
[3] K. Sun, Z. Gu, H. Katsura, and S. Das Sarma, Phys. Rev. Lett. **106**, 236803 (2011).
[4] E. Tang, J.-W. Mei, and X.-G. Wen, Phys. Rev. Lett. **106**, 236802 (2011).
[5] T. Neupert, L. Santos, C. Chamon, and C. Mudry, Phys. Rev. Lett. **106**, 236804 (2011).
[6] Y.-F. Wang, Z.-C. Gu, C.-D. Gong, and D. N. Sheng, Phys. Rev. Lett. **107**, 146803 (2011).
[7] D. Sheng, Z.-C. Gu, Gu, K. Sun, and L. Sheng, Nat. Commun. **2**, 389 (2011).
[8] N. Regnault and B. A. Bernevig, Phys. Rev. X **1**, 021014 (2011).
[9] A. M. Läuchli, Z. Liu, E. J. Bergholtz, and R. Moessner, Phys. Rev. Lett. **111**, 126802 (2013).
[10] S. A. Parameswaran, R. Roy, and S. L. Sondhi, C. R. Phys. **14**, 816 (2013).
[11] E. J. Bergholtz and Z. Liu, Int. J. Mod. Phys. B **27**, 1330017 (2013).
[12] T. Neupert, C. Chamon, T. Iadecola, L. H. Santos, and C. Mudry, Phys. Scr. **T164**, 014005 (2015).
[13] F. D. M. Haldane, Phys. Rev. Lett. **61**, 2015 (1988).
[14] C.-Z. Chang, J. Zhang, X. Feng, J. Shen, Z. Zhang, M. Guo, K. Li, Y. Ou, P. Wei, L.-L. Wang, Z.-Q. Ji, Y. Feng, S. Ji, X. Chen, J. Jia, X. Dai, Z. Fang, S.-C. Zhang, K. He, Y. Wang *et al.*, Science **340**, 167 (2013).
[15] G. Jotzu, M. Messer, R. Desbuquois, M. Lebrat, T. Uehlinger, D. Greif, and T. Esslinger, Nature (London) **515**, 237 (2014).
[16] Z. Liu, E. J. Bergholtz, H. Fan, and A. M. Läuchli, Phys. Rev. Lett. **109**, 186805 (2012).
[17] Y.-F. Wang, H. Yao, C.-D. Gong, and D. N. Sheng, Phys. Rev. B **86**, 201101 (2012).
[18] S. Yang, Z.-C. Gu, K. Sun, and S. Das Sarma, Phys. Rev. B **86**, 241112 (2012).
[19] A. Sterdyniak, C. Repellin, B. A. Bernevig, and N. Regnault, Phys. Rev. B **87**, 205137 (2013).
[20] N. R. Cooper and J. Dalibard, Phys. Rev. Lett. **110**, 185301 (2013).
[21] N. Y. Yao, C. R. Laumann, A. V. Gorshkov, S. D. Bennett, E. Demler, P. Zoller, and M. D. Lukin, Phys. Rev. Lett. **109**, 266804 (2012).
[22] N. Y. Yao, A. V. Gorshkov, C. R. Laumann, A. M. Läuchli, J. Ye, and M. D. Lukin, Phys. Rev. Lett. **110**, 185302 (2013).
[23] A. Kumar and R. Nandkishore, Phys. Rev. B **87**, 241108 (2013).
[24] P. Ghaemi, J. Cayssol, D. N. Sheng, and A. Vishwanath, Phys. Rev. Lett. **108**, 266801 (2012).
[25] A. G. Grushin, A. Gómez-León, and T. Neupert, Phys. Rev. Lett. **112**, 156801 (2014).
[26] E. Sagi and Y. Oreg, Phys. Rev. B **90**, 201102 (2014).
[27] D. Xiao, W. Zhu, Y. Ran, N. Nagaosa, and S. Okamoto, Nat. Commun. **2**, 596 (2011).
[28] F. Wang and Y. Ran, Phys. Rev. B **84**, 241103 (2011).
[29] S. Kourtis, J. W. F. Venderbos, and M. Daghofer, Phys. Rev. B **86**, 235118 (2012).
[30] J. W. F. Venderbos, S. Kourtis, J. van den Brink, and M. Daghofer, Phys. Rev. Lett. **108**, 126405 (2012).
[31] J. W. F. Venderbos, M. Daghofer, and J. van den Brink, Phys. Rev. Lett. **107**, 116401 (2011).
[32] R. Liu, W.-C. Chen, Y.-F. Wang, and C.-D. Gong, J. Phys.: Condens. Matter **24**, 305602 (2012).
[33] W.-C. Chen, R. Liu, Y.-F. Wang, and C.-D. Gong, Phys. Rev. B **86**, 085311 (2012).
[34] X.-P. Liu, W.-C. Chen, Y.-F. Wang, and C.-D. Gong, J. Phys.: Condens. Matter **25**, 305602 (2013).
[35] S. Yang, K. Sun, and S. Das Sarma, Phys. Rev. B **85**, 205124 (2012).
[36] Y.-L. Wu, B. A. Bernevig, and N. Regnault, Phys. Rev. B **85**, 075116 (2012).

[37] T. Liu, C. Repellin, B. A. Bernevig, and N. Regnault, Phys. Rev. B **87**, 205136 (2013).
[38] B. A. Bernevig and N. Regnault, Phys. Rev. B **85**, 075128 (2012).
[39] Y.-F. Wang, H. Yao, Z.-C. Gu, C.-D. Gong, and D. N. Sheng, Phys. Rev. Lett. **108**, 126805 (2012).
[40] X. G. Wen and Q. Niu, Phys. Rev. B **41**, 9377 (1990).
[41] F. D. M. Haldane, Phys. Rev. Lett. **55**, 2095 (1985).
[42] R. Tao and F. D. M. Haldane, Phys. Rev. B **33**, 3844 (1986).
[43] R. B. Laughlin, Phys. Rev. B **23**, 5632 (1981).
[44] Q. Niu, D. J. Thouless, and Y.-S. Wu, Phys. Rev. B **31**, 3372 (1985).
[45] H. Li and F. D. M. Haldane, Phys. Rev. Lett. **101**, 010504 (2008).
[46] A. Sterdyniak, N. Regnault, and B. A. Bernevig, Phys. Rev. Lett. **106**, 100405 (2011).
[47] A. Sterdyniak, N. Regnault, and G. Möller, Phys. Rev. B **86**, 165314 (2012).
[48] A. G. Grushin, T. Neupert, C. Chamon, and C. Mudry, Phys. Rev. B **86**, 205125 (2012).
[49] C. Chamon and C. Mudry, Phys. Rev. B **86**, 195125 (2012).
[50] G. Murthy and R. Shankar, Phys. Rev. B **86**, 195146 (2012).
[51] S. Kourtis, T. Neupert, C. Chamon, and C. Mudry, Phys. Rev. Lett. **112**, 126806 (2014).
[52] S. M. Girvin, A. H. MacDonald, and P. M. Platzman, Phys. Rev. B **33**, 2481 (1986).
[53] S. A. Parameswaran, R. Roy, and S. L. Sondhi, Phys. Rev. B **85**, 241308 (2012).
[54] R. Roy, Phys. Rev. B **90**, 165139 (2014).
[55] E. Dobardžić, M. V. Milovanović, and N. Regnault, Phys. Rev. B **88**, 115117 (2013).
[56] T. Neupert, C. Chamon, and C. Mudry, Phys. Rev. B **87**, 245103 (2013).
[57] E. H. Lieb, Phys. Rev. Lett. **62**, 1201 (1989).
[58] M. Niţă, B. Ostahie, and A. Aldea, Phys. Rev. B **87**, 125428 (2013).
[59] C. Weeks and M. Franz, Phys. Rev. B **82**, 085310 (2010).
[60] A. Zhao and S.-Q. Shen, Phys. Rev. B **85**, 085209 (2012).
[61] N. Goldman, D. F. Urban, and D. Bercioux, Phys. Rev. A **83**, 063601 (2011).
[62] C. L. Kane and E. J. Mele, Phys. Rev. Lett. **95**, 226801 (2005).
[63] A. Stathopoulos and J. R. McCombs, ACM Trans. Math. Softw. **37**, 21:1 (2010).